Acta Geotechnica (2025) 20:2761–2778
https://doi.org/10.1007/s11440-024-02508-4

RESEARCH PAPER

Nanoscale interfacial tribology behavior between clay and sand: effects of cations, normal load and sliding velocity

Zhenyu He[1] · Yuan-Yuan Zheng[1] · Zhen-Yu Yin[2] · Pengchang Wei[2]

Received: 18 October 2023 / Accepted: 13 December 2024 / Published online: 17 January 2025

Abstract
The interfacial tribology between clay and sand could significantly affect the mechanical stability of soil structures, while it remains unclear in the microscale. In this study, molecular dynamics (MD) simulation method has been employed to investigate the nanoscale friction behavior between quartz and montmorillonite at dry state, where quartz and montmorillonite are the common components of sand and clay, respectively. The effects of normal load, interlayer cations, and sliding velocity on their frictional behavior were discussed. The simulation results indicated that the stick–slip effect during friction process was gradually weakened with the increasing sliding velocity or decreasing normal load. The shear stress increased with the increasing normal load, exhibiting an approximately linear relationship. The order of friction coefficients of montmorillonite-quartz with different interlayer cations was $Ca^{2+} > Zn^{2+} > Ni^{2+} > Pb^{2+} > Li^{+} > Rb^{+} > Cs^{+} > K^{+}$, illustrating that the friction coefficient of montmorillonite-quartz systems with divalent cations was greater than that with monovalent cations. The friction angle of montmorillonite-quartz with different interlayer cations varies from 6.96 to 17.28°. Moreover, the friction load rose linearly with the sliding velocity, indicating that nanoscale friction was velocity-dependent.

Keywords Clay · Interfacial friction · Interlayer cation · Molecular dynamics · Montmorillonite · Sand

1 Introduction

Clay and sand are among the most common soil types, widely used in various geotechnical engineering projects including foundations and underground structures. These soils often coexist and interact, generating frictional forces that significantly affect the mechanical stability of soil structures. Additionally, the frictional behavior between clay and sand is crucial in various engineering fields, such as nuclear waste disposal and geothermal energy extraction. Quartz is a common component of sand, while montmorillonite is a prevalent clay mineral for its low frictional properties and high expansion capacity [21]. The mechanical properties of montmorillonite are significantly influenced by temperature, pressure, hydration state, cation type, and the presence of CO_2 [35]. Many geological disasters (e.g., earthquakes, faults, landslides, debris flows, etc.) are usually caused by frictional/shear sliding between soil mineral particles [14]. For instance, the anomalous large slip (50–80 m) during the 2011 Tohoku earthquake was attributed to the presence of a soft clay layer (e.g., montmorillonite) within the fault zone [13, 52]. Therefore, a thorough understanding of the friction behavior at the quartz-montmorillonite interface is crucial for advancements in soil mechanics and engineering design.

So far, the friction behavior of clay and sand is typically investigated through experiments, such as triaxial shear tests, rotational shear friction tests [16, 26], and biaxial friction tests [49]. These studies indicated that the temperature [26], hydration state [49], normal load [34], and interlayer cations [3, 49] can significantly influence their frictional properties at the macroscale. However, most macroscale friction studies have primarily focused on

✉ Pengchang Wei
pengchang.wei@polyu.edu.hk

[1] School of Civil Engineering, Sun Yat-Sen University & Southern Marine Science and Engineering Guangdong Laboratory (Zhuhai), Zhuhai 519082, China

[2] Department of Civil and Environmental Engineering, The Hong Kong Polytechnic University, Hung Hom, Kowloon, Hong Kong, China

individual quartz or montmorillonite samples. On the other hand, the frictional characteristics of quartz and montmorillonite mixtures was also investigated. For example, Ikari et al. [19] conducted shear tests on soil samples composed of mixtures of calcium montmorillonite powder and quartz sand in various proportions. Saffer et al. [40] investigated the frictional behavior of different ratios of montmorillonite and quartz through laboratory tests. Li et al. [28] developed a cohesion model for saturated montmorillonite-quartz remolded soil under acid rain conditions, finding that cohesion initially decreased, then increased, and ultimately decreased again. Tembe et al. [48] examined the frictional behavior of clay materials with quartz under stress conditions. These studies have significantly contributed to understanding the frictional characteristics of montmorillonite and quartz mixtures. However, a detailed understanding of the nanoscale tribology of soil at the microscale remained unclear, especially the interfacial friction of montmorillonite and quartz. These gaps limit our ability to develop comprehensive models for accurately predicting friction across different scales.

In macroscopic experiments, it is challenging to reveal the interfacial friction mechanisms of materials. On the other hand, the nanoscale tribology studies can uncover the fundamental friction mechanisms [17]. In the late twentieth century, the rapid development of nanoscience and technology has enabled extensive exploration of mechanical phenomena from macro- to nanoscale. Nanotribology [4], a branch of tribology, has made significant advances in theory, experimentation, and simulation. Techniques such as friction force microscopy [18], optical microscopy, and scanning electron microscopy have been used to study the friction properties of various materials [19]. Molecular dynamics (MD) simulation method becomes a versatile tool in nanotribology for exploring the dynamic processes of structural changes and providing atomic-level information of materials [20], such as asphalt, polymers, and graphene [18, 51, 59]. However, the study of nanoscale friction in soil/rock remained limited.

Wei et al. investigated the nanoscale interfacial friction of hydrated montmorillonite [56] and quartz-kaolinite system [55] through MD simulation method, considering normal load, sliding velocity, hydration, etc. They revealed the fundamental friction mechanism of soil and discussed the stick–slip effect. Xu et al. [60] utilized MD simulations to investigate the interfacial friction behavior of quartz under various factors, including normal load, water lubrication, and surface orientation. To identify the origins of molecular and macroscopic friction, Sakuma et al. studied the nanoscale friction behavior of mica surfaces [41] and montmorillonite with different cations [42] through density functional theory calculations and direct shear tests. Abbasi et al. [1] examined the effects of hydration and hydrostatic stress on the sliding mechanisms of sodium montmorillonite using MD simulations. Ying et al. [61] discussed the effect of ion type and concentration on the frictional behavior of montmorillonite. However, studies on the interfacial friction behavior of mixtures of different geomaterials at the nanoscale are still scarce, particularly for the interface between quartz and montmorillonite.

In this work, the steered molecular dynamics (SMD) simulation method was employed to investigate the nanoscale tribology between montmorillonite and quartz, considering the effects of normal load, interlayer cation, and sliding velocity. The frictional mechanism of dry montmorillonite-quartz and its structural properties were discussed. The friction angles of montmorillonite-quartz concerning different interlayer cations and sliding velocities were obtained to compare with previous work. Moreover, the evolution of total energy, pairwise interaction energy, and potential of mean force (PMF) were discussed. This work aims to gain an in-depth understanding of the frictional behavior at the nanoscale interface between montmorillonite and quartz, thereby providing new perspectives and theoretical foundations for tribological research at the macroscopic scale.

2 Simulation details

2.1 System setup

Montmorillonite is the primary mineral in bentonite, comprising 50% to over 90% of its composition, whereas the quartz content is relatively low. In this study a montmorillonite-quartz model (see Fig. 1) was established to facilitate computational feasibility and to uncover the fundamental interfacial mechanisms at the molecular level. As shown in Fig. 1, the Ca-montmorillonite-quartz interface model consists of a quartz slider and montmorillonite substrate, where the unit cell of montmorillonite and quartz model was derived from Viani et al. [53] and Levien et al. [27], respectively. Moreover, the accuracy of the montmorillonite model used in this work was verified in our previous work [57] through comparison with other experimental and simulation studies. It was worth noting that eight montmorillonite-quartz models with different interlayer cations were established, such as Ca^{2+}, Zn^{2+}, Ni^{2+}, Pb^{2+}, Li^{+}, Rb^{+}, Cs^{+}, and K^{+}. The quartz slider (10a × 7b × 4c, containing 3547 atoms) and montmorillonite substrate ($20a \times 10b \times 2c$, containing 18,994 atoms) were established, and their lattice parameters are shown in Fig. 1a. The simulation box dimensions were 103.6 Å × 89.8 Å × 69.2 Å, including a vacuum of about 30 Å in the z-direction, to avert the interaction between the neighboring upper and lower portions of montmorillonite

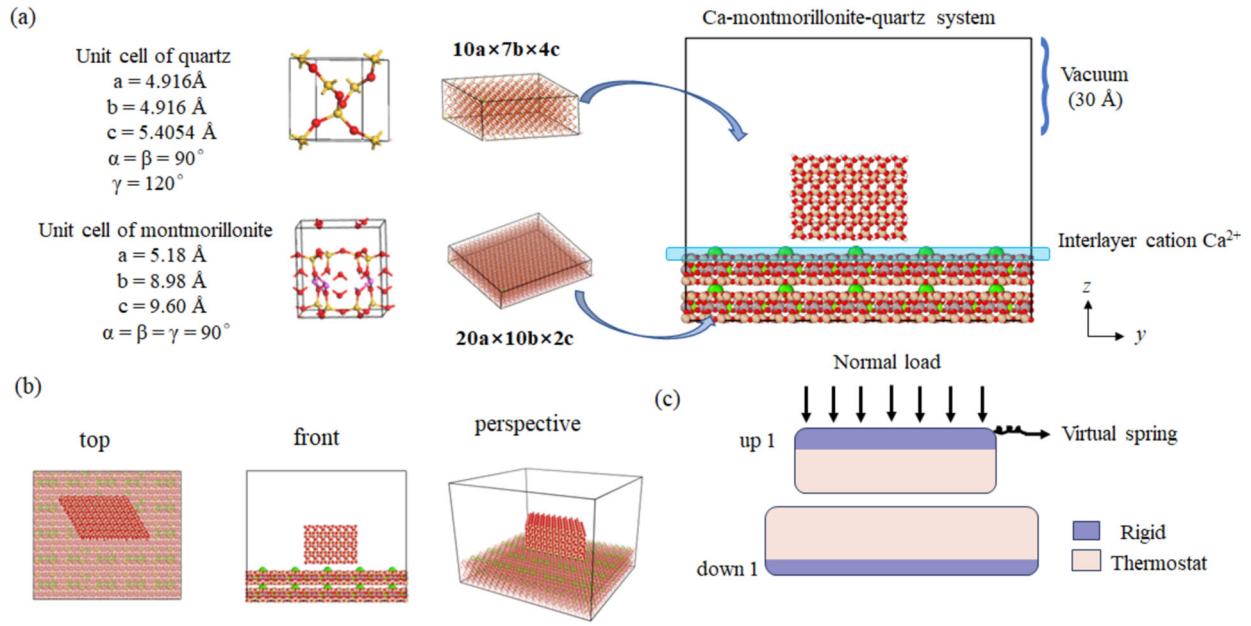

Fig. 1 **a** Ca-montmorillonite-quartz model used in this work, where quartz is set as slider and montmorillonite as substrate. **b** The whole system is shown in three views: top, front, and perspective. **c** The setting way of the whole system in this work: purple portions (containing *up1* and *down1*) are rigid in all directions, where *up1* could move along *y*-direction by a virtual spring and be applied by a normal load, pink portions are set as thermostat to control the temperature of the whole system

due to the periodicity of the *z*-direction. The area of the loading surface (equal to the shear surface) was the area of the *xy* plane of the quartz slider.

The whole simulation model was divided into two portions, the rigid portion (purple) and the thermal control portion (pink), as shown in Fig. 1c. The *down1* and *up1* sheets were set as rigid bodies (purple), where the *up1* sheet transferred the external normal loads on the clay-quartz system without structural deformation, and the *down1* sheet was fixed in its position during the whole simulation. All other portions except up1 and down1 were set as temperature-controlled layers (pink) to keep the system at a target temperature. Those layers are free to move during the simulation process. Moreover, the same normal load was applied on each atom of the *up1* sheet perpendicular to the clay mineral layers, and a virtual spring was applied on the *up1* sheet to provide a constant sliding velocity along the *y*-direction ([010] crystal orientation). At the same time, this virtual spring was used to measure the friction load between the quartz slider and montmorillonite substrate, where a stiffness coefficient of 100 N/m was employed to ensure reliability and save computational costs [56].

2.2 Force field

All MD simulations were adopted using the Large-scale Atomic/Molecular Massively Parallel Simulator (LAMMPS) package [37]. CLAYFF [9] force field was applied in whole models, which has been used for clay minerals [7, 11, 30] and quartz-kaolinite systems [32, 55] in MD simulations. The force field parameter of montmorillonite-quartz system was mainly derived from the literature [9], where their Lennard–Jones parameters are listed in Table 1. The force field parameters of interlayer cations used in this work were all derived from previous research and have been extensively validated. For example, the structure and energetic parameters of cesium ion-water clusters have been investigated using MD simulation and a polarizable interaction model [43]. The total potential energy was calculated by Eq. (1).

Periodic boundary conditions were used in all three directions to simulate the behavior of macroscale systems. A Lennard–Jones potential function with a cut-off radius of 10 Å and the velocity Verlet algorithm [12] was conducted to solve the equations of motion. Long-range electrostatic interactions were calculated using the Ewald method [10] with a cut-off radius of 8.5 Å and an accuracy of 1.0e−6 kcal/mol. The steered molecular dynamics (SMD) simulation method was initially performed in bio-molecule simulations and has been utilized broadly to explore the interface interactions at the atomic scale. So far, the SMD simulation method has been gradually used to study the nanoscale friction behavior of materials [54, 60], where a moving spring force to a group of atoms can be applied. The virtual spring can be controlled in either constant force or velocity mode to induce transitions in the systems [36].

Table 1 Lennard–Jones parameters of montmorillonite-quartz system applied in this work

Species	Symbol	Charge	ε(kcal/mol)	σ(Å)	References
Hydroxyl hydrogen	Ho	0.425	0	0	Cygan et al. [9]
Hydroxyl oxygen	Oh	− 0.95	0.1554	3.1655	
Bridging oxygen	Ob	− 1.05	0.1554	3.1655	
Bridging oxygen with octahedral substitution	Obos	− 1.1808	0.1554	3.1655	
Bridging oxygen with tetrahedral substitution	Obts	− 1.1688	0.1554	3.1655	
Hydroxyl oxygen with substitution	Ohs	− 1.0808	0.1554	3.1655	
Tetrahedral silicon	Si	2.1	1.8405×10^{-6}	3.3020	
Octahedral aluminum	Al (ao)	1.575	1.3298×10^{-6}	4.2713	
Tetrahedral aluminum	Al (at)	1.575	1.8405×10^{-6}	3.3020	
Octahedral magnesium	Mg	1.36	9.0298×10^{-7}	5.2643	
Aqueous sodium ion	Na^+	1	0.1301	2.35	Smith and Dang [43]
Aqueous potassium ion	K^+	1	0.1000	3.7423	Koneshan et al. [24]
Aqueous cesium ion	Cs^+	1	0.1000	4.3002	Smith and Dang [43]
Aqueous lithium ion	Li^+	1	0.164	1.505	Smith and Dang [44]
Aqueous rubidium ion	Rb^+	1	0.04	4.114	Rappe et al.[39]
Aqueous calcium ion	Ca^{2+}	2	0.1000	2.869	O.Steinhauser [45]
Aqueous nickel ion	Ni^{2+}	2	0.015	2.834	Prasanth et al. [38]
Aqueous zinc ion	Zn^{2+}	2	0.124	2.763	Rappe et al. [39]
Aqueous lead ion	Pb^{2+}	2	0.663	4.297	Rappe et al. [39]

The snapshots of the model were obtained from OVITO software [46].

$$E_{\text{total}} = E_{\text{bond stretch}} + E_{\text{angle bend}} + E_{\text{Coulomb}} + E_{\text{VDW}} \quad (1)$$

where $E_{\text{bond stretch}}$, $E_{\text{angle bend}}$, E_{Coulomb}, and E_{VDW} are bond stretch energy, angle bend energy, coulombic energy, and van der Waals energy, respectively. Only the bond of oxygen and hydrogen (in water or hydroxyl) was included in the bond stretch energy.

$$E_{\text{bond stretch}} = k_1\left(r_{ij} - r_0\right)^2 \quad (2)$$

$$E_{\text{angle stretch}} = k_2\left(\theta_{ijk} - \theta_0\right)^2 \quad (3)$$

where k_1 is force constant, r_0 represents the equilibrium bond length, both taken from the flexible version of the SPC water model, and r_{ij} is the distance between atoms i and j. Only the hydrogen–oxygen–hydrogen angle in the water molecule was considered in the angle bend energy, where k_2 is force constant, θ_{ijk} is the bond angle of hydrogen–oxygen–hydrogen, and θ_0 represents the equilibrium bond angle.

$$E_{\text{VDW}} = 4\varepsilon_{ij}\left[\left(\frac{\sigma_{ij}}{r_{ij}}\right)^{12} - \left(\frac{\sigma_{ij}}{r_{ij}}\right)^{6}\right] \quad (4)$$

$$E_{\text{Coulomb}} = \frac{e^2 q_i q_j}{4\pi\varepsilon_0 r_{ij}} \quad (5)$$

where q_i and q_j are the charges of atoms i and j, respectively, ε_0 is the dielectric constant. σ and ε are the size and energy parameters, respectively. Moreover, σ_{ij} and ε_{ij} can be obtained by Mixing Lorentz-Berthelot law [40], as shown in Eqs. (6) and (7).

$$\sigma_{ij} = \frac{\sigma_i + \sigma_j}{2} \quad (6)$$

$$\varepsilon_{ij} = \sqrt{\varepsilon_i \varepsilon_j} \quad (7)$$

2.3 Relaxation and SMD friction process

To obtain a fully balanced configuration of the montmorillonite-quartz system, the simulation scheme is carried out as follows, shown in Table 2. (1) Firstly, the geometry optimization of the entire system was performed using energy minimization with the conjugate gradient (CG) methods. Convergence criteria were determined with an energy tolerance of 1.0e−12, a force tolerance to 1.0e−14 kcal (mol Å)$^{-1}$, and a maximum number of iterations to 1000. (2) First relaxation: the whole system equilibrated in canonical (NVT) ensemble at 300 K for 1000 ps, where the Langevin algorithm with a damping parameter of 100 was utilized to maintain the system's

Table 2 SMD simulation schemes for montmorillonite-quartz system in this work

Steps	Relaxation and Steered molecular dynamics (SMD) simulation process	
1	Energy minimization	Conjugate Gradient (CG.) Algorithm
2	First relaxation	NVT ensemble relaxation for 1000 ps
3	Second relaxation	NVT ensemble, Langevin temperature control (300 K), different normal loads: 1–8 GPa, relaxation for 400 ps
4	SMD friction simulation	NVT ensemble, Langevin temperature control (300 K), conducting SMD friction simulation along the *y*-direction under various constant sliding velocities and normal loads of 1–8 GPa, then obtaining a sliding distance of approximately 100 Å
		The run time is calculated based on the total sliding distance and the set sliding velocity

temperature. (3) Second relaxation: the temperature of the thermal control sheet (pink) was controlled at 300 K using the Langevin algorithm. Simultaneously, different normal loads (1–8 GPa) were applied to the atoms of *up1* sheet (purple) in the NVT ensemble for 400 ps. (4) Thereafter, SMD friction simulations were conducted along the *y*-direction for all montmorillonite-quartz systems under various constant sliding velocities and normal loads of 1–8 GPa. A virtual spring with a stiffness coefficient of 100 N/m was employed. Moreover, the run time for the SMD friction simulation varied with sliding velocity, covering a consistent sliding distance of approximately 100 Å. For example, the run time was 200 ps at a sliding velocity of 50 m/s.

3 Results and discussion

The friction behavior of soil or rock in the nanoscale is affected by factors such as normal load, sliding velocity, interlayer cations, hydration, temperature. In this work, Sect. 3.1 discusses the influence of normal loads of 1–8 GPa on the friction behavior of the Ca-montmorillonite-quartz interface at a sliding velocity of 50 m/s. Section 3.2 shows the effect of different interlayer cations, including monovalent and divalent cations, such as Ca^{2+}, Zn^{2+}, Ni^{2+}, Pb^{2+}, Li^{+}, Rb^{+}, Cs^{+}, and K^{+}, on the friction behavior of montmorillonite-quartz under a normal load of 1-8 GPa and a sliding velocity of 50 m/s. Section 3.3 explore the impact of various sliding velocities (1–1000 m/s) on friction properties of Ca-montmorillonite-quartz interface, focusing on velocity-dependent sliding in nanoscale tribology. Finally, Sect. 3.4 summarizes the connection between macroscale and nanoscale friction, highlighting the underlying mechanisms.

3.1 Influence of normal load

3.1.1 Structural evolution

To investigate the structural wearing situation during friction process, the trajectory diagrams of the Ca-montmorillonite-quartz system at normal loads of 1, 5, and 8 GPa in periodic and non-periodic conditions are displayed in Fig. 2. At a normal load of 1–5 GPa, the molecular morphology of the contact surface exhibited inapparent changes when the quartz slider slid on montmorillonite substrate (Fig. 2a–d). However, at a normal load of 8 GPa, only a tiny part of the quartz slider remains intact (Fig. 2e and f), whereas a large majority of molecules in the quartz slider have collapsed during the period. These atoms wear under high normal loads during the friction process, leaving on the montmorillonite surface.

Moreover, Fig. 3a displays the structure diagrammatic sketch of the quartz slider under the normal load from 1 to 8 GPa both from the side and top views, where the quartz slider is destroyed and some collapsing molecules widely distributed on the montmorillonite surface under normal load of 7 and 8 GPa. The remaining height of the quartz slider under different normal loads is shown in Fig. 3b, where the remaining height of the quartz slider reduces with rising normal loads. Therefore, we only consider the normal load of less than 6 GPa in this work.

3.1.2 Friction load evolution and stick–slip effect

The evolution of friction load with sliding distance in Ca-montmorillonite-quartz at different normal loads is shown in Fig. 4a. During the sliding process, the friction load presented a periodic crenelated wave phenomenon at different normal loads, indicating that the stick–slip effect [33] also existed in nanoscale friction between montmorillonite and quartz. The fluctuation amplitude of the friction load increased with increasing normal load, showing a more significant stick–slip effect, as shown in Fig. 4a. As the quartz portion slides, the distance between the adjacent surface atoms changed, resulting in changes in the interaction between these atoms. The higher the normal load, the higher the friction load because more energy was required to overcome the interaction between montmorillonite and quartz.

As shown in Fig. 4b, the average shear stress [56] increases with the rising normal load, where their relationship is approximately linear. Wei et al. [55] also reported that the relationship between normal load and

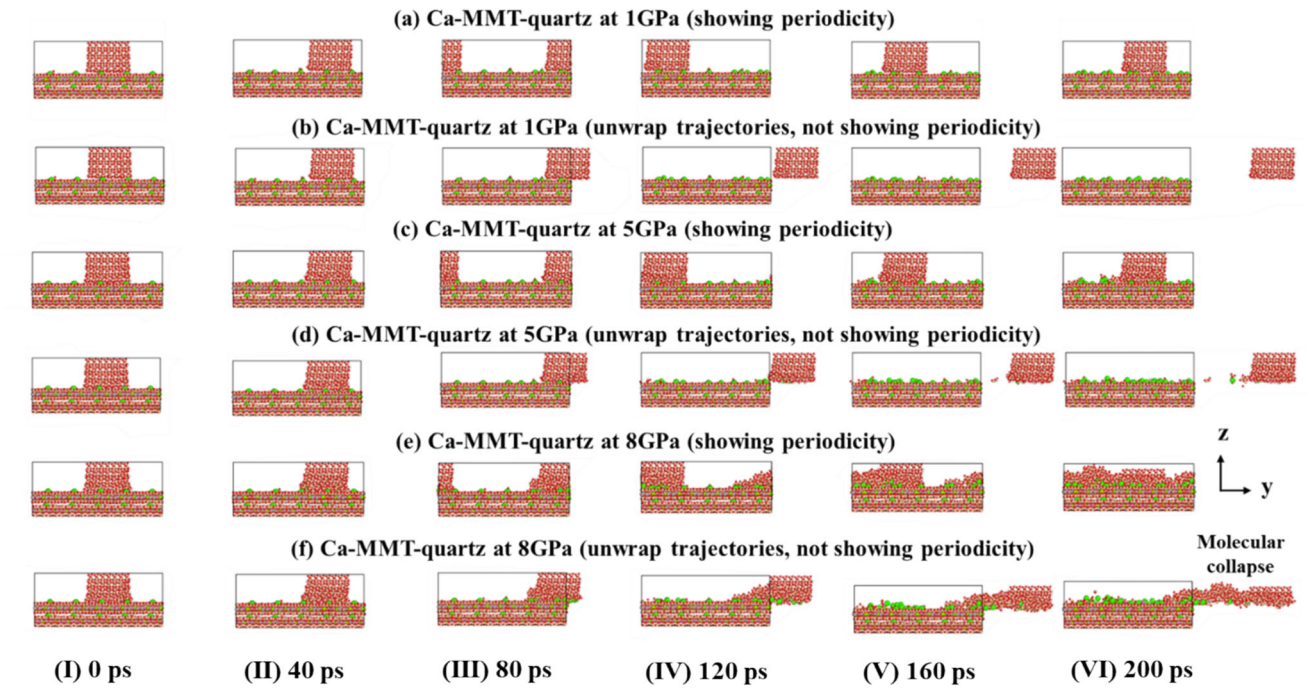

Fig. 2 Trajectory diagram of Ca-montmorillonite-quartz under different normal loads of **a**, **b** 1 GPa; **c**, **d** 5 GPa; **e**, **f** 8 GPa during the whole simulation, with the interval of the output images is 40 ps. The sliding velocity is 50 m/s, and the temperature is 300 K

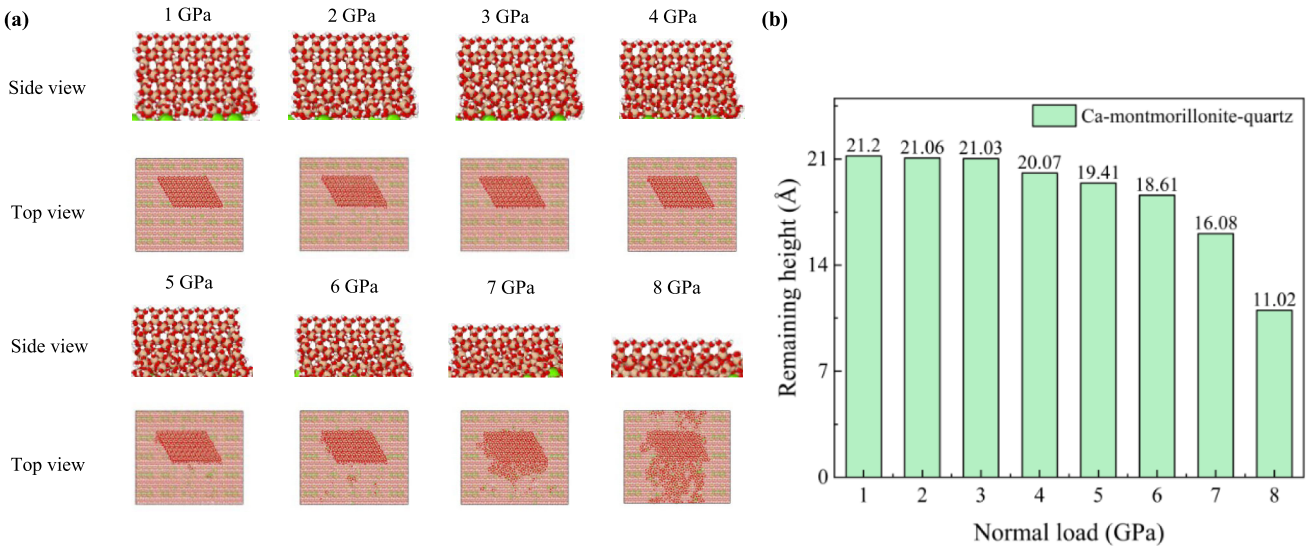

Fig. 3 **a** The structure diagrammatic sketch of quartz slider under different normal loads from side and top view after friction. **b** The evolution of the remaining height of quartz with normal load. Moreover, the initial height along z-direction of quartz slider without normal load was 21.6216 Å

friction load (shear stress) of soil or rock at the nanoscale was approximately linear.

The friction coefficient (μ) can be obtained via Eq. (8),

$$f = \mu F_n + F_0 \qquad \tau = \mu \sigma_n + c \tag{8}$$

where f is the friction load, μ the friction coefficient, F_n is the applied normal load, and the cohesion F_0 is the vertical intercept when $F_n = 0$. The shear stress τ and normal load σ_n are obtained from the average friction load and normal load divided by the shear area of the sliding block, and c is the cohesion.

On the other hand, the key factors leading to the stick–slip effect in the nanoscale can be summarized as surface roughness and topography, temperature, material properties like elasticity and plasticity, load and pressure, sliding

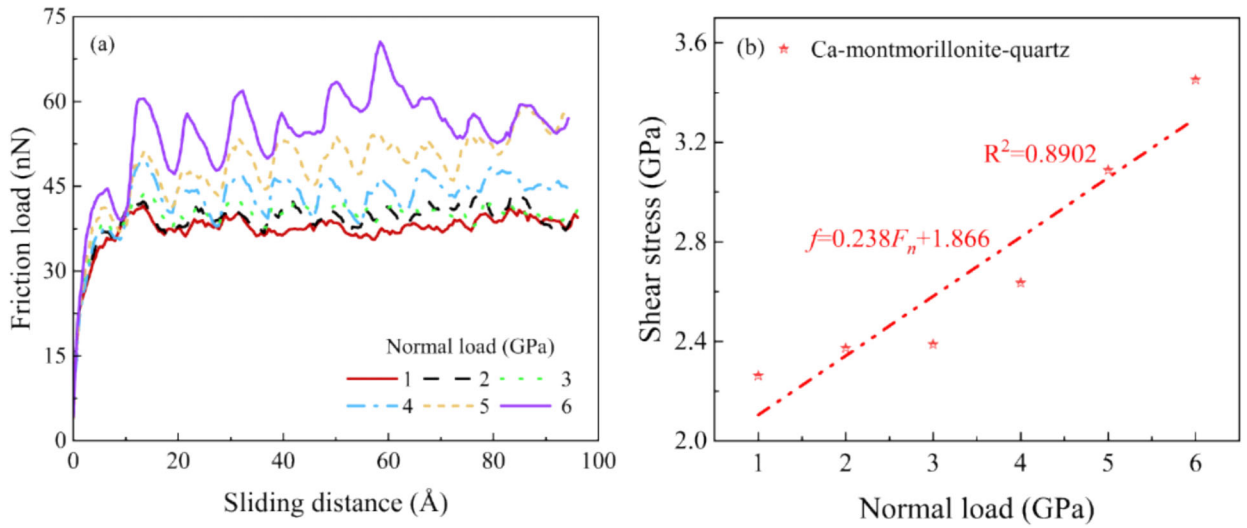

Fig. 4 The friction behavior for Ca-montmorillonite-quartz model: **a** evolution of the friction load with sliding distance at different normal loads and a constant sliding velocity of 50 m/s. Moreover, **b** evolution of average shear stress with different normal loads of Ca-montmorillonite-quartz, where the average shear stress (i.e., average friction load divided by shear surface area) was averaged based on the data during sliding distance range of 50–100 Å

velocity, intermolecular interactions, etc. [2, 6, 50, 61] The interfacial interaction between montmorillonite and quartz in MD simulation was mainly non-bonded interaction (i.e., intermolecular interaction), including coulombic interaction and van der Waals interaction, which was crucial for the stick–slip effect.

The nanoscale mechanism in the stick–slip effect can be attributed to the adsorption and desorption processes between surface atoms. When two solid surfaces come into contact, adhesion forces dominate, causing the surfaces to stick together. Subsequently, as an external force is applied, the surfaces begin to slide while this adhesive force is still acting until it reaches a critical threshold. Once this threshold is overcome, surface atoms rapidly desorb, leading to the momentary interruption of sliding, which is the characteristic feature of the stick–slip phenomenon [25]. Based on the previous work [42, 58], the potential energy surface (PES) of materials, as a reflection of intermolecular interaction and crystal structure, plays an essential role in the stick–slip effect.

To explore the correlation between PES and the stick–slip effect, one interlayer cation as a probe atom, positioned 2 Å above the interlayer cations, was employed to scan a particular line of montmorillonite surface, with the scanning path illustrated in Fig. 5a, d. Figure 5b, e showed the variation of friction load with sliding distance for both monovalent (M^+) and divalent (D^{2+}) interlayer cations systems, with the period of stick–slip effect 8.1 Å and 16.9 Å for M^+-mmt-quartz and D^{2+}-mmt-quartz systems, respectively. The arrangement period of potential energy value in the shear direction (y-direction) was 8.1 Å and 16.9 Å for M^+-mmt and D^{2+}-mmt, align with the period of stick–slip motion, as shown in Fig. 5c and f. Therefore, it could be determined that the stick–slip effect is tightly linked to the potential energy of interlayer cations and montmorillonite surface.

3.1.3 Potential of mean force and energy evolution

The potential of mean force (PMF) describes the average distribution of the potential energy of intermolecular interactions on a multidimensional free energy surface. PMF is the criterion of the spontaneous process, which could be obtained from the thermodynamic integration of the system based on Jarzynski's equation as follows:

$$\mathrm{PMF} = -\frac{1}{k_{\mathrm{B}}T}\log\left(e^{-\frac{W}{k_{\mathrm{B}}T}}\right) \tag{9}$$

where W, k_{B}, and T are the work of spring, Boltzmann constant, and system temperature, respectively.

As shown in Fig. 6, the PMF increases linearly with the increase in sliding distance, and the slope of the PMF-sliding distance curve increases with rising normal load, indicating further that more energy is required at higher normal loads during the sliding process. Besides, as shown in Fig. 7, the total energy of the whole system exponentially increases with the rising normal load during the second relaxation process and SMD friction process, where total energy in the SMD friction simulation process rises more rapidly than that in the second relaxation process.

The evolution of the total energy increment with time under different normal loads for the Ca-montmorillonite-quartz system is investigated at a sliding velocity of 50 m/s, as shown in Fig. 8. In the second relaxation process, total

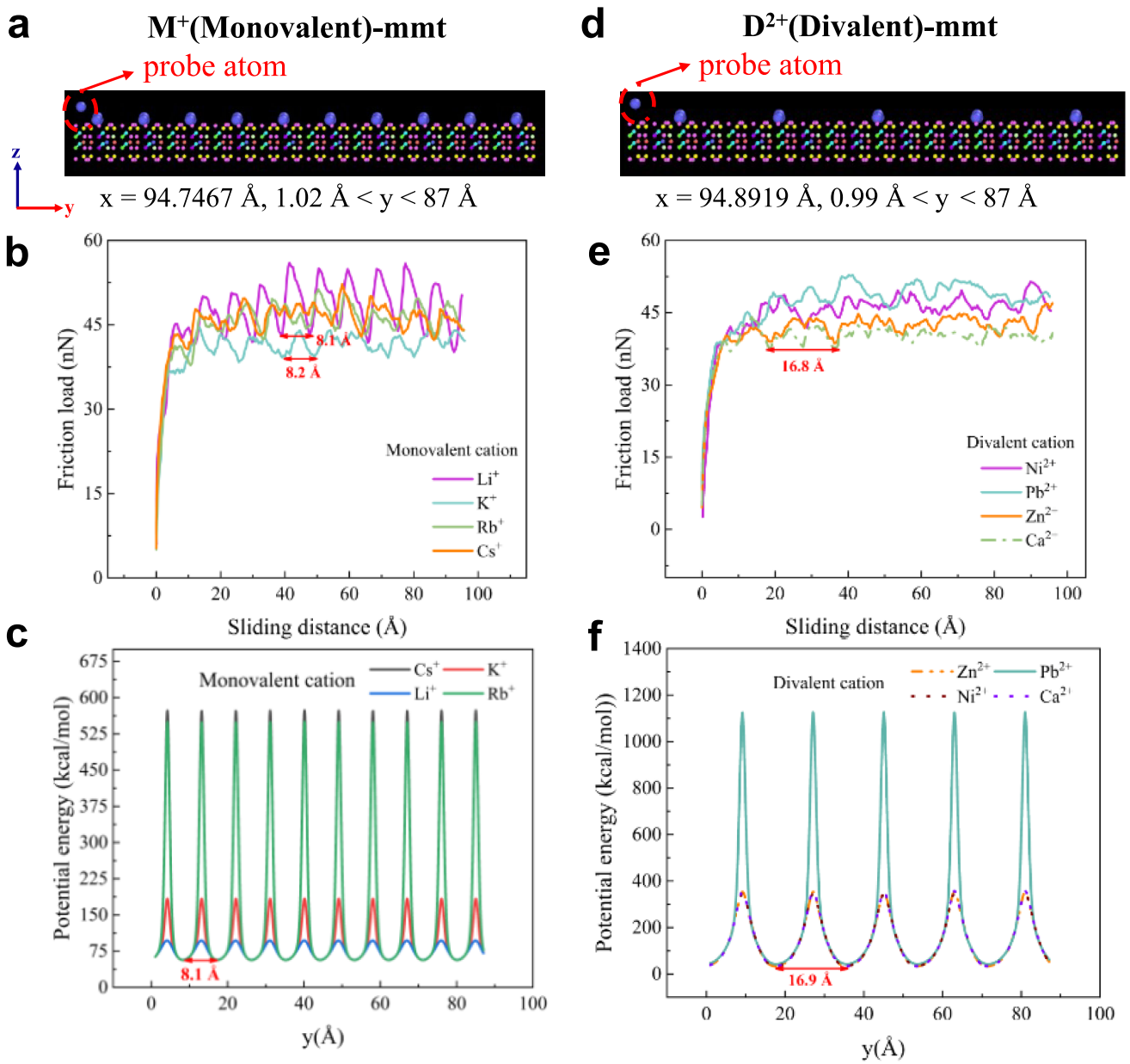

Fig. 5 Investigation for the relationship between stick–slip phenomenon and potential energy in terms of different interlayer cations of montmorillonite: Initial structure of **a** M^+(Monovalent)-mmt and **d** D^{2+}(Divalent)-mmt when calculating the potential energy, with a probe ion in the upper left corner; evolution of friction load and sliding distance of **b** M^+-mmt-quartz and **e** D^{2+}-mmt-quartz systems at 3 GPa; potential energy varies for **c** M^+-mmt and **f** D^{2+}-mmt

energy fluctuates around a value throughout the period where the energy of whole system is relatively stable, as shown in Fig. 8a. Meanwhile, it could be easily figured out that the bigger the normal load, the higher the total energy is in the system. On the other hand, Fig. 8b displays the evolution of the total energy increment with time during SMD friction simulation process. At the normal load superior or equal to 4 GPa, the total energy rose gradually with time, indicating that more continuous energy was required for the whole system during friction.

Pairwise interaction energy was calculated to analyze the interaction of two atom groups. The higher the absolute value of pairwise interaction energy, the more significant the interaction between these two groups. Figure 9 and Table 3 show the evolution of pairwise interaction energy between the montmorillonite and quartz group and their pairwise interaction force, respectively. As shown in Fig. 9 and Table 3, the higher the normal load, the higher the absolute value of pairwise interaction energy and force, illustrating that the interaction between montmorillonite

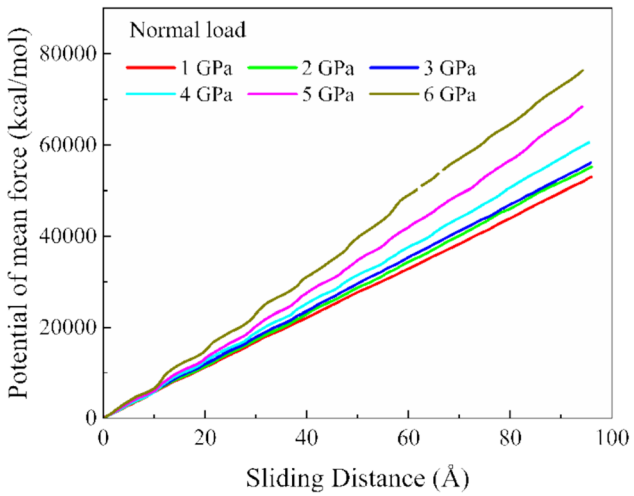

Fig. 6 Evolution of correspondence of mean force (PMF) potential with sliding distance under different normal loads

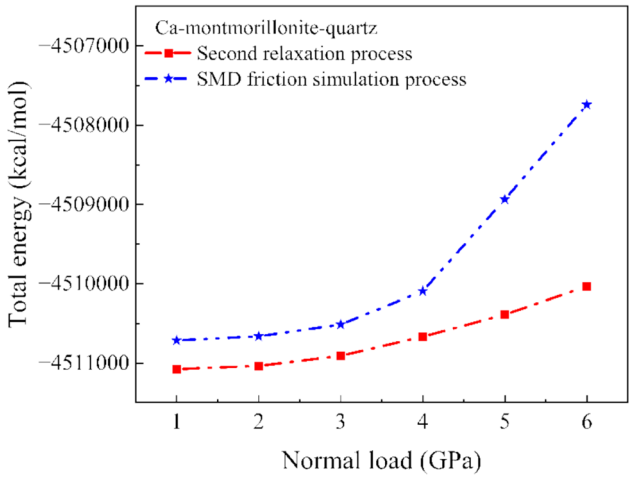

Fig. 7 The effect of normal load on the total energy of the whole system during the second relaxation process (red line) and SMD friction process (blue line). The total energy is taken from the average of the second half of the simulation

and quartz increases with rising normal load. The increment of normal load could affect the interaction between the sliding block and substrate, which originated from intermolecular forces and the normal load applied on the quartz slider.

3.2 Influence of interlayer cations

3.2.1 Effect of cation valence and radius

To investigate the influence of interlayer cations on the friction properties of montmorillonite-quartz system, eight different cations were considered in this work. The evolution of the shear stress with normal loads for montmorillonite-quartz systems with different interlayer cations is shown in Fig. 10, where their relationship is approximately linear, agreed well with previous studies [55, 56, 59, 60].

Based on Eq. (8), the friction coefficient and cohesion of montmorillonite-quartz system with different interlayer cations are obtained in Fig. 11. As shown in Fig. 11, the order of friction coefficients for montmorillonite-quartz systems with different interlayer cations is $Ca^{2+} > Zn^{2+} > Ni^{2+} > Pb^{2+} > Li^{+} > Rb^{+} > Cs^{+} > K^{+}$, illustrating that the friction coefficients of divalent cations system are greater than that of monovalent cations system. The higher friction strength observed in this work containing divalent cations was primarily due to stronger electrostatic attractions, reduced interlayer spacing, increased structural rigidity, smaller ionic radius, higher polarizability, and stronger interfacial interactions with quartz, which collectively contribute to the increased resistance to shear strength systems with divalent cations [20, 47].

Table 4 shows the relationship between the interlayer cation radius and friction coefficient of this work and comparison with previous studies, where their relationship and fundamental mechanism are very complex and controversial according to previous works. Sakuma et al. [42] reported that the shear strength increased with the ionic radius of interlayer cations through DFT and shear experiments for dehydrated montmorillonite. However, Ying et al. [61] found the opposite trend for a hydration case using MD simulation. Theoretically, the larger ions did not fit in the ditrigonal cavities, resulting in the greater sliding resistance due to the electrostatic repulsion between interlayer ions and clay surface. Moreover, Ying et al. [61] observed that the hydrated cation sizes order ($K^{+} < Na^{+} < Ca^{2+} < Mg^{2+}$) is the reverse of the effective ionic radius order [31], indicating that montmorillonite with different interlayer cations had varying water absorption and swelling behavior in a hydration state. The friction coefficient of materials was jointly regulated by surface adhesion and hydration of cations [5].

To sum up, this study focused on the interfacial friction of dry montmorillonite substrate and quartz slider, but there were inevitable differences between different substrates and slider materials. Although the correlation between cation radius/hydration and friction coefficient of soil has been studied, they were still controversial and needed to be investigated in future.

Table 5 displays the friction coefficient, cohesion, and friction angle of various quartz-montmorillonite (Mt) interfaces in this work and previous studies. The friction angle and friction coefficient of montmorillonite-quartz with monovalent cations were smaller than that with divalent cations, while the cohesion showed the opposite trend. Moreover, the friction coefficient decreases with the increasing sliding velocities. As shown in Table 5, at 300 K and sliding velocity of 100 m/s, the order of fiction

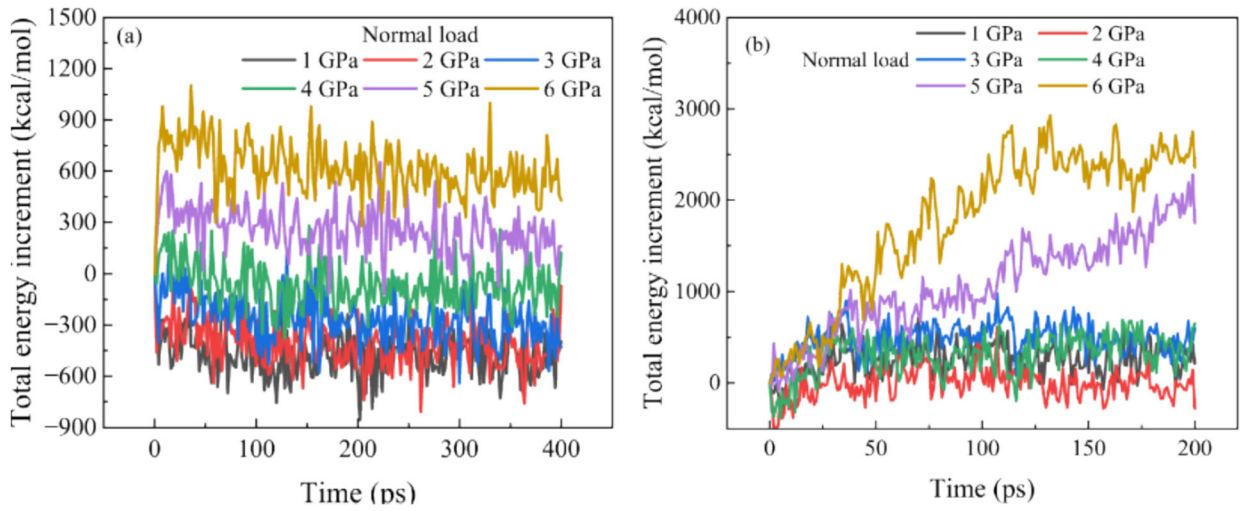

Fig. 8 The evolution of total energy increment of Ca-montmorillonite-quartz system with time under different normal loads: **a** during the second relaxation process; **b** during the SMD friction process. The total energy increment is the difference between the total energy during the sliding process and the initial total energy in the beginning of the sliding process (t = 0 ps)

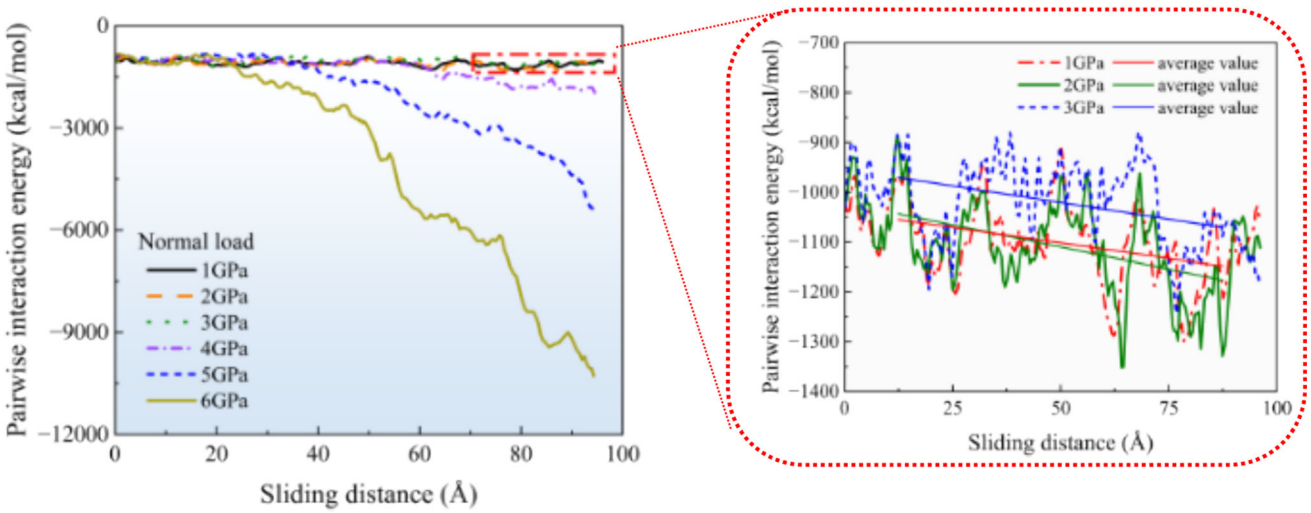

Fig. 9 The evolution of pairwise interaction energy between Ca-montmorillonite and quartz group under different normal loads. The right figure magnifies the 1–3 GPa curve in the left figure, and straight lines were fitted from the data which was averaged at intervals of 25 Å

coefficient of various quartz-clay systems in MD simulation is quartz-quartz (0.270) > Ca-montmorillonite-quartz (0.176) > quartz-kaolinite (0.044). Meanwhile, Tembe et al. [48] and Saffer et al. [40] also found that the presence of clay weakens the frictional strength of quartz through conventional triaxial tests.

3.2.2 Energy evolution

The evolution of total energy with normal loads in different quartz-montmorillonite systems with various interlayer cations is shown in Fig. 12, where the Rb^{2+} curve is the highest, but Ni^{2+} occupies the lowest position. The total energy grew as the normal load increased for eight cation groups. Except for the Pb-montmorillonite-quartz, Fig. 12 indicates that the total energy of the whole system with divalent cations like Ca^{2+}, Zn^{2+}, and Ni^{2+} are less than that with monovalent cations.

To understand the interaction between quartz slider and montmorillonite substrate with various interlayer cations, the pairwise interaction energy was calculated to understand the stability of the system and the interaction between each other. Figure 13 shows that all pairwise interaction energy gradually declines with rising normal loads, especially at normal loads of 6–8 GPa.

Table 3 Pairwise interaction energy and its force between Ca-montmorillonite and quartz group at the end of the sliding process (t = 200 ps)

Normal load (GPa)	Pairwise interaction energy (kcal/mol)	Pairwise interaction force (nN)			
		x-direction	y-direction	z-direction	total
1	− 1058.4	− 3.8644	6.5493	− 21.2904	7.5359
2	− 1111.11	− 1.980	5.4763	− 36.0954	12.1874
3	− 1181.02	7.4872	12.5933	− 49.0597	17.0669
4	− 2041.46	5.2641	15.3418	− 63.0951	21.7155
5	− 5360.68	3.9770	20.4698	− 77.3355	26.6992
6	− 10,284.8	1.2239	22.7810	− 89.6529	30.8367

3.3 Influence of sliding velocity

According to the Coulomb law at the macroscale, the sliding velocity was independent of the friction load of materials. However, in the microscale, the sliding velocity played an essential role in the friction behavior of materials [29, 60, 62], and their relationship was very different and complex under certain conditions for various materials. In this work, several different velocities were considered in the interfacial friction of Ca-montmorillonite-quartz.

Figure 14 shows the relationship between friction load and sliding velocity under 1–200 m/s and 60–80 Å. At the sliding velocity of less than 200 m/s, the friction load keeps fluctuating. Still, it is relatively stable over the period, agreeing with the stick–slip and adhesion phenomenon in nanoscale tribology [2, 8, 50], as shown in Fig. 14b. However, Fig. 14a exhibits that the friction load increases during the simulation process when the sliding velocity is over 200 m/s, which may be attributed to the continuous changes in the formation of atomic-scale junctions, the rearrangement of atoms and molecules under thermal activation or more different asperities on opposing surfaces [1, 2]. Moreover, kinds of surface chemistry and material properties could also increase friction load in various trends. Although the relationship between friction load and normal load is rather complex, further study will be conducted on the influencing mechanism of velocity in the friction surface.

The higher the sliding velocity, the higher the friction load, and the smaller the fluctuation amplitude of the friction load, illustrating the weaker the stick–slip effect, which agrees with previous studies about the stick–slip effect [50, 55].

Figure 15 displays the evolution of average friction load with sliding velocity at various sliding velocities, and their relationship is linear, which is in agreement with the result in the previous study [23], as shown in Eq. (10). Kheiri et al. [23] also found that the friction load linearly depends on the sliding velocity for aluminum spherical particle and graphene interface using MD simulation. The observed dependence starkly contrasts the macroscopic Amontons–

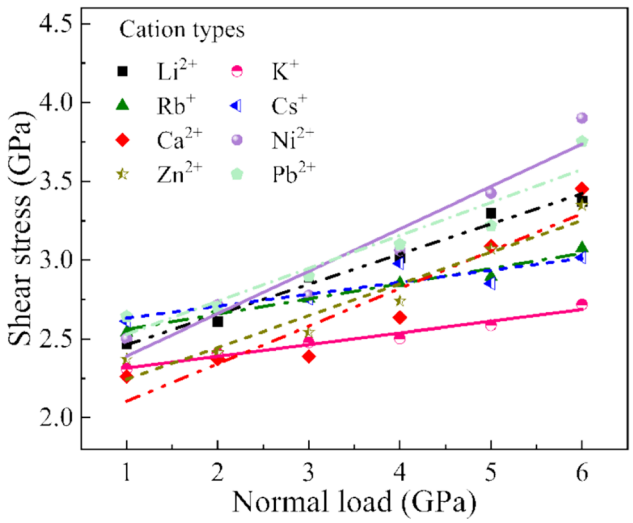

Fig. 10 Evolution of shear stress with normal load for montmorillonite-quartz interface with different interlayer cations under different normal loads

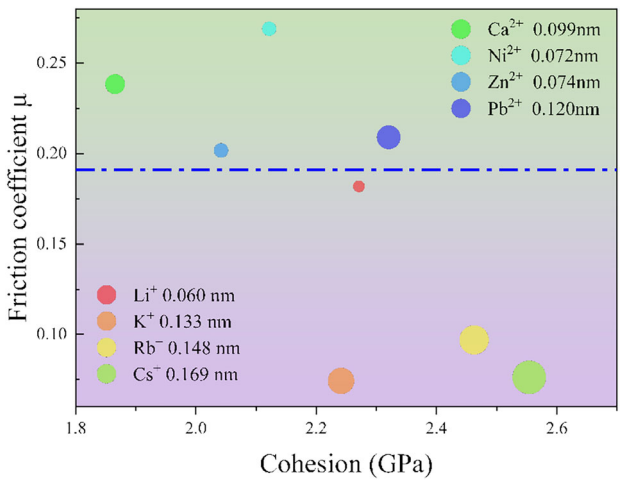

Fig. 11 The relationship of ionic radius, cohesion, friction coefficient (μ), and the circle size represents the radius size of the corresponding cations

Table 4 The correlation of cation radius of interlayer cation in montmorillonite and friction coefficient/strength in this work and comparison with some previous studies

System and methods	Friction coefficient/strength	References
Hydrated montmorillonite using MD	K^+ (0.133 nm) < Na^+ (0.095 nm) < Ca^{2+} (0.099 nm) < Mg^{2+} (0.065 nm)	Ying et al. [61]
Partial dehydration montmorillonite using DFT and experiment	Li^+ (0.06 nm) < Na^+ (0.095 nm) < K^+ (0.133 nm) < Cs^+ (0.169 nm) < Rb^+ (0.148 nm)	Sakuma et al. [42]
Friction experiment of montmorillonite in a given humidity	Ca^{2+} (0.099 nm) < Na^+ (0.0095 nm)	Tetsuka et al. [49]
Hydrate montmorillonite under triaxial shear test	Ca^{2+} (0.099 nm) = Mg^{2+} (0.065 nm) < Na^+ (0.095 nm) < K^+ (0.133 nm)	Behnsen and Faulkner [3]
Dry montmorillonite-quartz using MD	K^+ (0.133 nm) < Cs^+ (0.169 nm) < Rb^+ (0.148 nm) < Li^+ (0.06 nm) < Pb^{2+} (0.120 nm) < Ni^{2+} (0.072 nm) < Zn^{2+} (0.074 nm) < Ca^{2+} (0.099 nm)	This work

Table 5 The friction coefficient, cohesion, and friction angle of various quartz-montmorillonite (Mt) interfaces in this work and previous studies

Interface of soil particles or mixtures of clay-quartz	Method	Friction angle (°)	Friction coefficient	Cohesion (GPa)	Notes
Li-Mt-quartz	MD simulation in this work	10.31	0.182	2.271	300 K, 50 m/s
K-Mt-quartz		4.24	0.0741	2.242	
Rb-Mt-quartz		5.53	0.0968	2.463	
Cs-Mt-quartz		4.35	0.0761	2.5547	
Ca-Mt-quartz		13.41	0.2384	1.8657	
Ni-Mt-quartz		15.1	0.269	2.122	
Zn-Mt-quartz		11.42	0.202	2.042	
Pb-Mt-quartz		11.81	0.209	2.321	
Ca-Mt-quartz		18.16	0.328	− 0.239	300 K, 1 m/s
		13.44	0.239	0.277	300 K, 10 m/s
		10.09	0.178	2.994	300 K, 80 m/s
		9.98	0.176	3.679	300 K, 100 m/s
		8.47	0.149	4.408	300 K, 120 m/s
		7.35	0.129	5.364	300 K, 150 m/s
		7.41	0.130	6.289	300 K, 180 m/s
		6.22	0.109	6.893	300 K, 200 m/s
Quartz-quartz [55]	MD simulation	15.96	0.286	0.255	200 K, 100 m/s
		15.11	0.270	0.233	300 K, 100 m/s
		14.90	0.266	0.184	400 K, 100 m/s
Quartz grains [22]	Experiment test	11.86	0.21	–	300 K
Quartz sand [7]	Shear stress	5.31–13.01	0.093–0.231	–	300 K
Quartz-water-quartz [55]	MD simulation	5.37	0.094	0.215	300 K, 100 m/s
Quartz-kaolinite [55]		2.52	0.044	0.402	300 K, 100 m/s
Quartz-water-kaolinite [55]		4.80	0.084	0.263	300 K, 100 m/s
Smectite [40]	Laboratory experiment	4.00–16.70	0.07–0.30	–	300 K, 150 μm/s
Smectite-quartz mixtures [40]		11.31–27.92	0.2–0.53	–	300 K, 150 μm/s
					Smectite-quartz mixtures ranging from 10 to 90% quartz
Illite shale [40]		22.29–32.21	0.41–0.63	–	300 K, 150 μm/s
Quartz (95%)-Mt (5%) mixtures [48]	The conventional triaxial tests	33.06	0.651	–	Room temperature, effective normal stress of 40 MPa
Quartz (85%)-Mt (15%) mixtures [48]		32.09	0.627	–	
Quartz (75%)-Mt (25%) mixtures [48]		24.47	0.455	–	

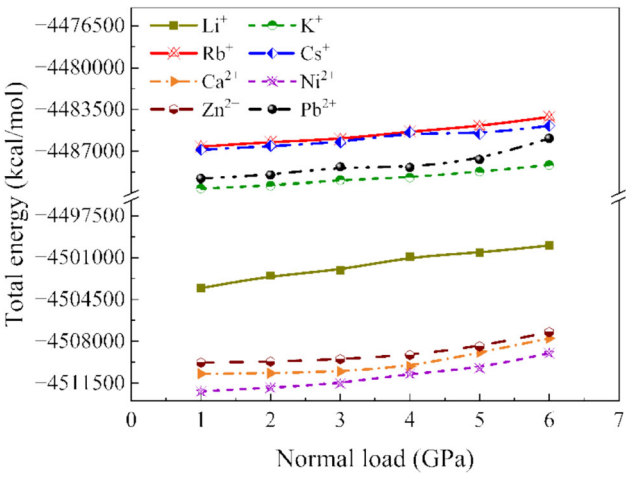

Fig. 12 Evolution of total energy with normal load for montmorillonite-quartz with different cations

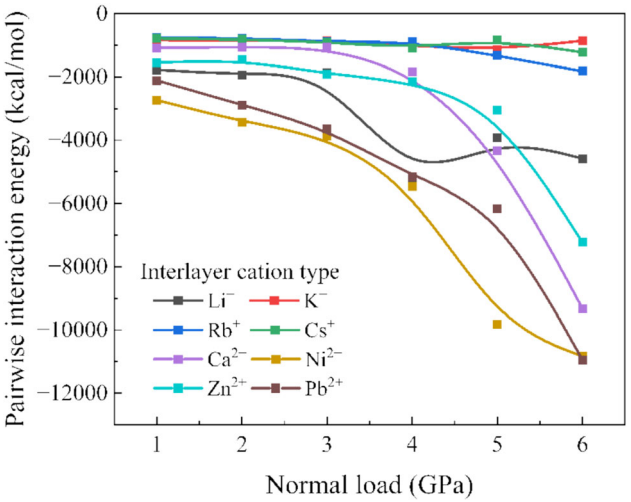

Fig. 13 Evolution of Pairwise interaction energy of montmorillonite-quartz with different cations with normal load

Coulomb laws, which anticipate the velocity independence of sliding friction [23].

Moreover, the simulation result in this work differed from the non-linear dependence of sliding velocity and friction load from the PT model. Although the similarity of our simulation data with the predictions of the PT model was not expected, the primary reason for the difference may be the relatively large sliding velocities used in our study [23].

$$F_{\mathrm{fr}} = \gamma v \tag{10}$$

where γ is the friction coefficient, v is the sliding velocity, and F_{fr} is the friction load. This is a non-dimensional equation.

The Prandtl–Tomlinson (PT) model reported less time for the tip to hop out from the barrier due to thermal activation under a higher velocity, resulting in higher friction. The relationship between average friction and sliding velocity based on the PT model is shown in Eq. (11) [15].

$$F_k = F_L^* + \frac{k_{\mathrm{B}}T}{\lambda}\ln\frac{v}{v_1} \tag{11}$$

where F_k is the average Friction, $F_L{}^*$ is the reference force needed to make the energy barrier vanish at zero temperature, k_{B} is the Boltzmann constant, T is the temperature, λ is a parameter for describing the speed the energy barrier to the next slip event vanishes with increasing lateral force, v_1 is the reference velocity, existing because of the uniformity of the scale and can usually be taken directly as 1 for simplicity, in the same units as v.

To explore the effect of sliding velocity on the frictional behavior of Ca-montmorillonite-quartz interface, the relationship of shear stress and normal load at 1–200 m/s is shown in Fig. 16. The friction coefficient and cohesion declined with increasing sliding velocities, which agreed well with the work of Logan and Rauenzahn [31], who also reported negative velocity dependency in pure quartz and a slight positive velocity dependency of other gauges through experiment.

Figure 17 displays a perspective on the changing value of potential energy and kinetic energy increment, with their sum representing the total energy increment of the system. The higher the sliding velocity, the higher the thermal motion of the molecules and the more changes in their relative positions, reflecting higher potential and kinetic energy. Figure 18 displays the structure diagrammatic of the Ca-montmorillonite-quartz system in different velocities under the normal load of 3 GPa. When the sliding velocities were less than 200 m/s, the structure of the whole system remained unchanged. However, when the sliding velocities were over 200 m/s, the connection bond of the upper part of the quartz was broken, leading to damage to the structure. It indicated that the crystal structure of the slider could easily undergo wear and damage at higher sliding velocities. Thus, in SMD friction simulation, the sliding velocity was suggested to be less than 200 m/s to avoid the whole system deformation.

3.4 Discussion on nanoscale and macroscale friction mechanism

The macroscale friction behavior of materials usually follows the classical friction theory, which states that the friction force is independent of the sliding velocity and is proportional to the normal load. Moreover, the macroscale friction properties of geo-materials are primarily influenced by several factors, including surface roughness, contact area, and the presence of water or other fluids. For instance,

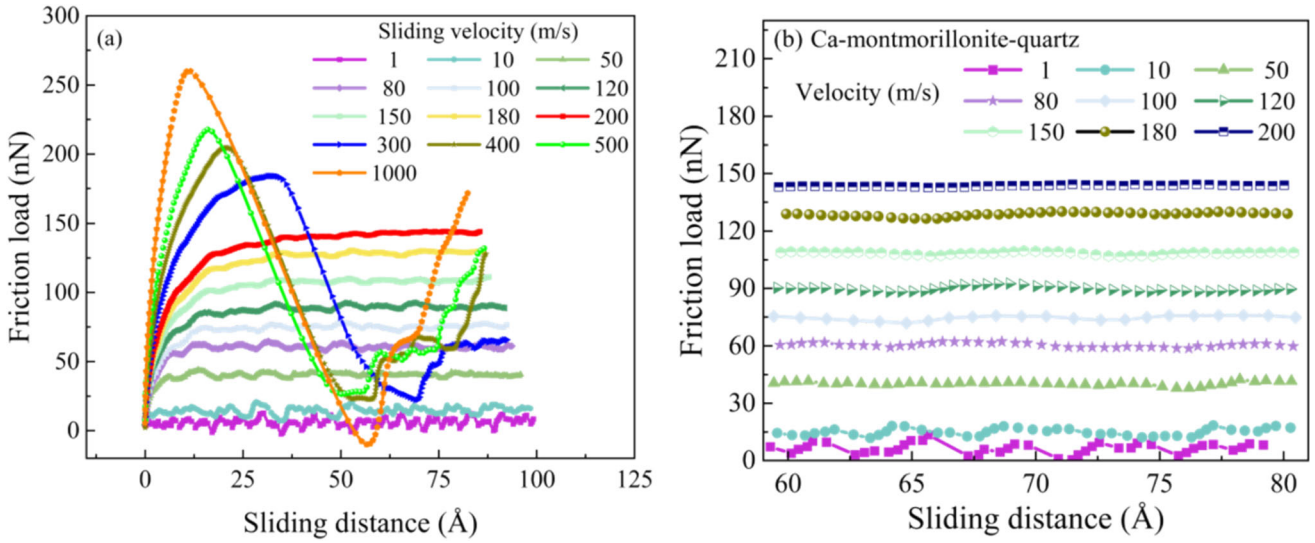

Fig. 14 The friction load as a function of sliding distance at various velocities under normal load of 3 GPa in Ca-montmorillonite-quartz system

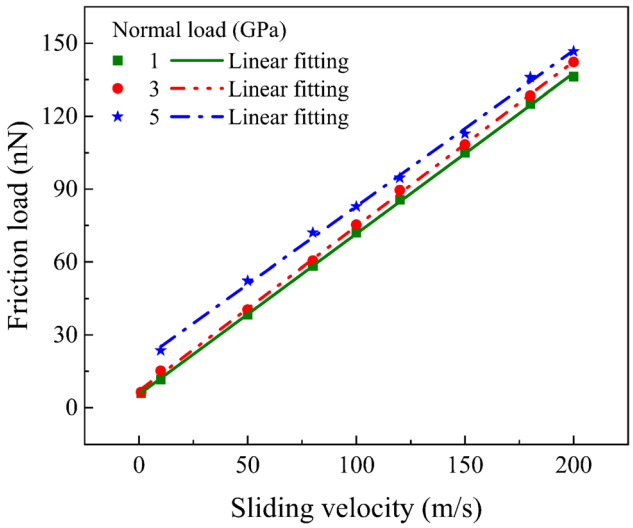

Fig. 15 Friction load versus sliding velocity under normal load of 1, 3 and 5 GPa in Ca-montmorillonite-quartz system

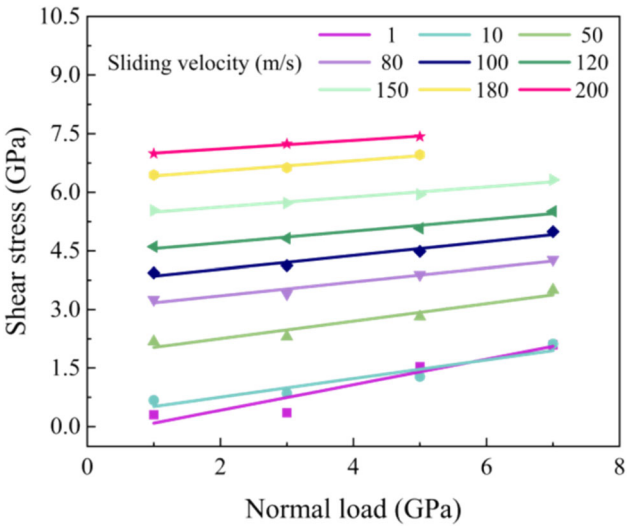

Fig. 16 Evolution of shear stress with normal load for Ca-montmorillonite-quartz interface under different sliding velocities of 1–200 m/s

water molecules can form a lubricating layer between quartz and montmorillonite, significantly reducing the friction coefficient.

In this work, for the nanoscale friction of quartz-montmorillonite system, the linear relationship between friction load and normal load, the complex correlation between cations and friction properties, and velocity-dependent in nanoscale friction were found. Nanoscale tribology of geomaterials was also related to water content, temperature, materials surface, ion concentration, etc. [18, 34, 55, 58]. Moreover, the stick–slip effect observed in this MD simulation and previous FFM experiments [33] at the microscale was closely associated with the potential energy surface of the materials and other influencing factors (e.g., normal load, sliding velocity, hydration, temperature, etc. [42, 55, 58]). However, the stick–slip effect was not exhibited on the macroscale.

To sum up, the nanoscale and macroscale friction have similarities and differences, where the similarities included the normal load effect, and the differences contained the sliding velocity effect, the stick–slip effect, etc. Furthermore, the nanoscale friction could provide an atomistic insight into the friction mechanism of materials, considering various environmental factors.

The connection between macroscopic and microscopic friction was crucial and discussed as follows: (1) The macroscopic friction behavior of a material is the integrated result of countless microscopic frictions.

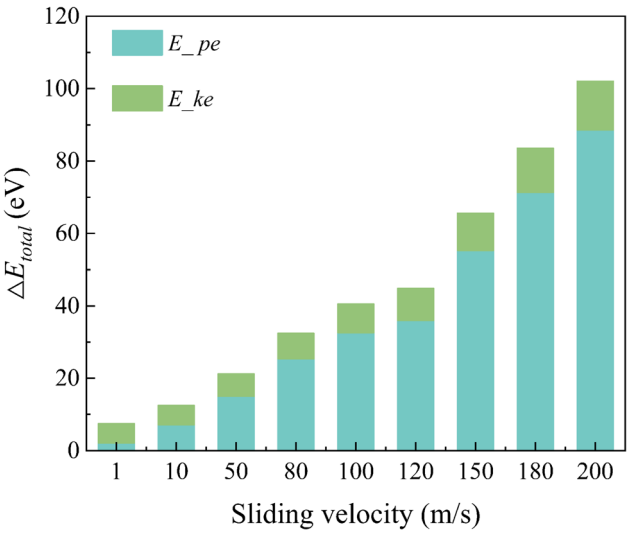

Fig. 17 The average potential and kinetic energy increment at various sliding velocities under 3 GPa normal load, with their sum value representing the total energy depicted on the vertical axis. The energy increment is the difference between the average value of the whole simulation and the initial value when the timestep is 0 ps

Fundamentally, the frictional force at the macroscale was the sum of many tiny forces acting at the atomic and molecular scale. The intermolecular interactions (including Van der Waals interaction, electrostatic interaction, etc.) of materials were significant at the nanoscale, collectively affecting the macroscopic frictional force. (2) The apparent contact area was important in the macroscale, but the true contact area at the microscale (i.e., the sum of the contact areas of all asperities) was what contributed to microscale friction [42, 57]. Therefore, as the asperities surface deformed at the microscopic scale, more contact points were created, which increased the actual contact area and ultimately affected the macroscopic friction. (3) The stick–slip effect was caused by the adhesion and sliding processes between atoms, which manifest macroscopically as friction force fluctuations and friction coefficient variations. (4) Although the nanoscale friction behavior of geomaterials has been gradually investigated, the nanoscale friction cannot simply scale up to macroscale friction, and the friction coefficient in the microscale could not be directly compared to that in the macroscale [56]. Thus, most studies for the connection between microscale and macroscale friction will be worth investigating in future.

4 Conclusion

The molecular dynamics simulation method was employed to investigate the nanoscale interfacial friction behavior between montmorillonite and quartz, considering the effect of normal loads, interlayer cation genres, and sliding velocities. This study provides novel insights into the interfacial friction of the montmorillonite-quartz system and explores the friction mechanisms of clay-sand interactions under various influencing factors, bridging the gap between macroscopic and micro/nanscale perspectives. The key conclusions are summarized as follows:

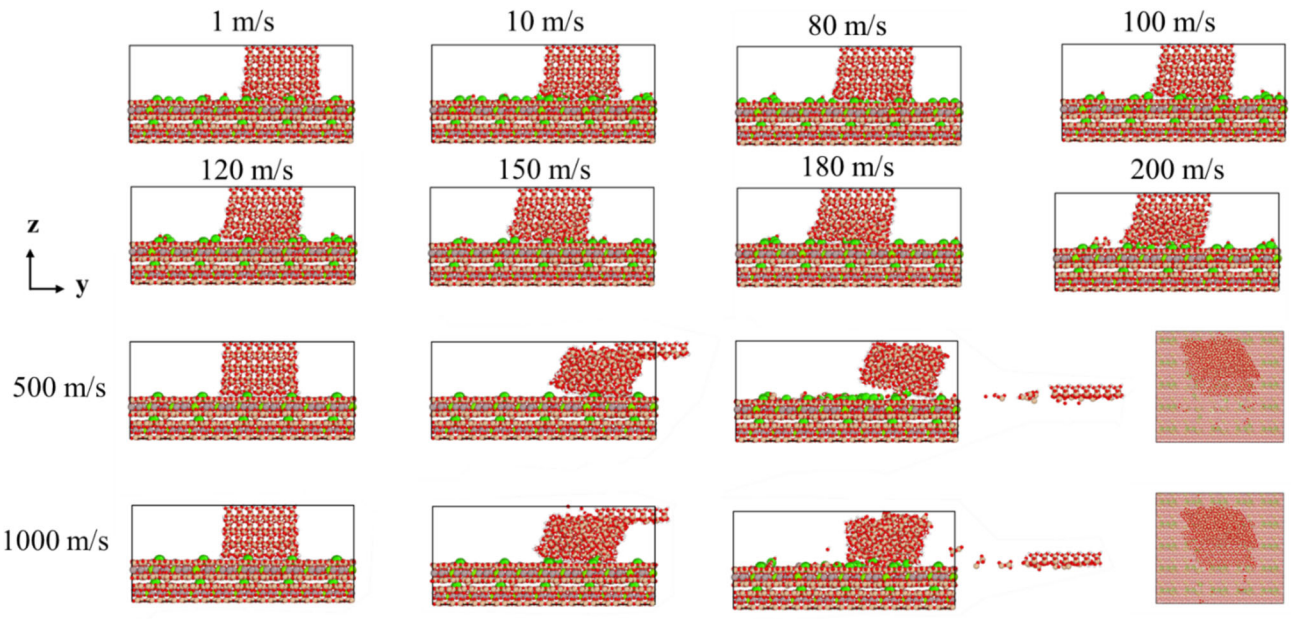

Fig. 18 The structure diagrammatic sketch of the quartz slider in different sliding velocities under the normal load of 3 GPa from the side and top view. When the sliding velocity is 1–200 m/s, the wearing condition of the structure is inapparent, while the upper part of the quartz slider is destroyed under higher sliding velocities (500 m/s and 1000 m/s). The trajectory diagrams are given for the 500 m/s and 1000 m/s plots

1. The order of friction coefficients of montmorillonite-quartz with different interlayer cations was Ca^{2+} > Zn^{2+} > Ni^{2+} > Pb^{2+} > Li^{+} > Rb^{+} > Cs^{+} > K^{+}, illustrating that the friction strength of montmorillonite-quartz system with divalent cations was greater than that of monovalent cations.
2. The friction load fluctuated with rising sliding distance during the whole sliding process, and the fluctuation amplitude increased with the upswing normal load, reflecting the stick–slip effect. The higher the sliding velocity or the lower the normal load, the weaker the stick–slip effect. The stick–slip phenomenon was highly related to the potential energy surface of materials.
3. The nanoscale friction at the montmorillonite-quartz interface was velocity-dependent, which was different from the macroscopic Amontons–Coulomb laws. Moreover, the friction coefficient of Ca-montmorillonite-quartz decreased with the rising sliding velocities. The average shear stress and normal load followed a roughly linear relationship.
4. The friction angle and friction coefficient of montmorillonite-quartz with different interlayer cations systems were 4.24°–15.1° and 0.0741–0.269, respectively.

The fundamental mechanisms by which the interlayer cations influence friction behavior of soil, as well as the impact of hydration state on friction, remain controversial and warrant further investigation in the future. Moreover, the force field played an essential role in MD simulation results, where the other force fields used for quartz will be worth employed to study its mechanical properties, such as CVFF, INTERFACE, and Tersoff force field. Most studies on the connection between microscale and macroscale friction will be worth investigating.

Acknowledgements This research is financially supported by National Natural Science Foundation of China (Grant No. 52009149), Natural Science Foundation of GuangDong Basic and Applied Basic Research Foundation (Grant No. 2021A1515012612), and the Research Grants Council (RGC) of Hong Kong Special Administrative Region Government (HKSARG) of China (Grant No. 15217220).

Author contributions Z-YH contributed to methodology, investigation, data curation, writing—review and editing, and writing—original draft; YZ contributed to writing—review and editing and project administration; Z-YY contributed to writing—review and editing and project administration; PWEI contributed to conceptualization, data curation, writing—review and editing, and supervision.

Funding Open access funding provided by The Hong Kong Polytechnic University.

Declarations

Conflict of interest The authors declare no competing interests.

References

1. Abbasi B, Muhunthan B, Salehinia I, Zbib HM (2020) Nanoscale stick-slip behavior of na-montmorillonite clay. J Eng Mech 146(12):4020138. https://doi.org/10.1061/(ASCE)EM.1943-7889.0001881
2. Balzer BN, Kienle S, Gallei M, von Klitzing R, Rehahn M, Hugel T (2014) Stick-slip mechanisms at the nanoscale. Soft Mater 12(sup1):S106–S114. https://doi.org/10.1080/1539445X.2014.945039
3. Behnsen J, Faulkner DR (2013) Permeability and frictional strength of cation-exchanged montmorillonite. J Geophys Res Solid Earth 118(6):2788–2798. https://doi.org/10.1002/jgrb.50226
4. Bhushan B, Kulkarni AV (1996) Effect of normal load on microscale friction measurements. Thin Solid Films 278(1):49–56. https://doi.org/10.1016/0040-6090(95)08138-0
5. Cai H, Zhang C, Li F, Liu M, Zhang T, Chu H, Liu Z (2023) Study on the microcosmic superlubricity mechanism of PVPA affected by metal cations. Friction 11(7):1150–1164. https://doi.org/10.1007/s40544-022-0632-7
6. Chen L, Zhang G, Chen Y (2010) Molecular dynamics simulation of stick-slip at nanoscale. J Southeast Univ (Nat Sci Ed) 40:128–132. https://doi.org/10.3969/j.issn.1001-0505.2010.01.024
7. Chen R, Liu X, Yang W, Xia Z, Kang X, Lushnikova A (2021) Wetting behavior of metakaolinite on the basal surfaces: molecular dynamics study. Comput Geotech 129:103863. https://doi.org/10.1016/j.compgeo.2020.103863
8. Chen W, Foster AS, Alava MJ, Laurson L (2015) Stick-slip control in nanoscale boundary lubrication by surface wettability. Phys Rev Lett 114(9):95502. https://doi.org/10.1103/PhysRevLett.114.095502
9. Cygan RT, Liang J, Kalinichev AG (2004) Molecular models of hydroxide, oxyhydroxide, and clay phases and the development of a general force field. J Phys Chem B 108(4):1255–1266. https://doi.org/10.1021/jp0363287
10. Darden T, York D, Pedersen L (1993) Particle mesh Ewald: an *N*·Log(N) method for Ewald sums in large systems. J Chem Phys 98(12):10089–10092. https://doi.org/10.1063/1.464397
11. Du J, Zhou A, Shen S, Lin X, Bu Y, Kodikara J (2022) Revealing crucial effects of temperature and salinization on swelling behavior of montmorillonite. Chem Eng J 429:132263. https://doi.org/10.1016/j.cej.2021.132263
12. Frenkel D, Smit B, Tobochnik J, McKay SR, Christian W (1997) Understanding molecular simulation. Comput Phys 11(4):351–354. https://doi.org/10.1063/1.4822570
13. Fulton PM, Brodsky EE, Kano Y, Mori J, Chester F, Ishikawa T, Harris RN, Lin W, Eguchi N, Toczko S (2013) Low coseismic friction on the Tohoku-Oki fault determined from temperature

measurements. Science 342(6163):1214–1217. https://doi.org/10.1126/science.1243641
14. Ghafari M, Nahazanan H, Yusoff ZM, Ghiasi V (2021) Effect of soil cohesion and friction angles on reverse faults. Earthq Eng Eng Vib 20(2):329–334. https://doi.org/10.1007/s11803-021-2023-x
15. Gnecco E, Bennewitz R, Gyalog T, Loppacher C, Bammerlin M, Meyer E, Güntherodt HJ (2000) Velocity dependence of atomic friction. Phys Rev Lett 84(6):1172–1175. https://doi.org/10.1103/PhysRevLett.84.1172
16. Hirono T, Tsuda K, Kaneki S (2019) Role of Weak materials in earthquake rupture dynamics. Sci Rep-UK 9(1):6604. https://doi.org/10.1038/s41598-019-43118-5
17. Hölscher H, Schirmeisen A, Schwarz UD (2008) Principles of atomic friction: from sticking atoms to superlubric sliding. Philos Trans R Soc A 366(1869):1383–1404. https://doi.org/10.1098/rsta.2007.2164
18. Hou Y, Zhang H, Wu J, Wang L, Xiong H (2018) Study on the microscopic friction between tire and asphalt pavement based on molecular dynamics simulation. Int J Pavement Res Technol 11(2):205–212. https://doi.org/10.1016/j.ijprt.2017.09.001
19. Ikari M, Saffer D, Marone C, Samuelson J (2006) Shear induced pore pressure generation in montmorillonite-based fault gouge. In: Saffer D (ed). Washington, D.C.
20. Israelachvili J (2011) Intermolecular and surface forces, 3rd ed
21. Jianhui L, Zhiqiang Y, Yuqi J, Hongyan Y, Chenyang C, Rui D (2022) Study on the mechanical properties of clayey slip zone soil considering montmorillonite content. https://doi.org/10.21203/rs.3.rs-2178907/v1
22. Kasyap SS, Senetakis K (2019) Experimental investigation of the coupled influence of rate of loading and contact time on the frictional behavior of quartz grain interfaces under varying normal load. Int J Geomech 19(10):4019112
23. Kheiri R, Tsukanov A, Brilliantov N (2022) The velocity dependence of dry sliding friction at the nano-scale
24. Koneshan S, Rasaiah JC, Lynden-Bell RM, Lee SH (1998) Solvent structure, dynamics, and ion mobility in aqueous solutions at 25 °C. J Phys Chem B 102(21):4193–4204. https://doi.org/10.1021/jp980642x
25. Krylov SY, Jinesh KB, Valk H, Dienwiebel M, Frenken JWM (2005) Thermally induced suppression of friction at the atomic scale. Phys Rev E 71(6):65101. https://doi.org/10.1103/PhysRevE.71.065101
26. Kubo T, Katayama I (2015) Effect of temperature on the frictional behavior of smectite and illite. J Miner Pet Sci 110(6):293–299. https://doi.org/10.2465/jmps.150421
27. Levien L, Prewitt CT, Weidner DJ (1980) Structure and elastic properties of quartz at pressure. Am Mineral 65(9–10):920–930
28. Li L, Liu J, Xu X (2021) Study on the mechanical effect and constitutive model of montmorillonite under the action of acid rain: a case study on montmorillonite-quartz remolded soil. Adv Civ Eng 2021:1–10. https://doi.org/10.1155/2021/6644411
29. Li Q, Dong Y, Perez D, Martini A, Carpick RW (2011) Speed dependence of atomic stick-slip friction in optimally matched experiments and molecular dynamics simulations. Phys Rev Lett 106(12):126101. https://doi.org/10.1103/PhysRevLett.106.126101
30. Liu Y, Zheng Y, Lin H, Wei P, Fan Q, Huang G, Meng D (2024) Calculation of contact angle via Young-Dupré equation with molecular dynamic simulation: kaolinite as an example. Colloids Surf A Physicochem Eng Asp 697:134469. https://doi.org/10.1016/j.colsurfa.2024.134469
31. Logan JM, Rauenzahn KA (1987) Frictional dependence of gouge mixtures of quartz and montmorillonite on velocity. Compos Fabr Tectonophys 144(1–3):87–108. https://doi.org/10.1016/0040-1951(87)90010-2
32. Lu M, Zheng Y, Yin Z (2024) From sedimentation to consolidation of kaolinite: a molecular dynamic study. Comput Geotech 170:106285. https://doi.org/10.1016/j.compgeo.2024.106285
33. Mate CM, McClelland GM, Erlandsson R, Chiang S (1987) Atomic-scale friction of a tungsten tip on a graphite surface. Phys Rev Lett 59(17):1942–1945. https://doi.org/10.1103/PhysRevLett.59.1942
34. Morrow CA, Moore DE, Lockner DA (2017) Frictional strength of wet and dry montmorillonite. J Geophys Res Solid Earth 122(5):3392–3409. https://doi.org/10.1002/2016JB013658
35. Narayanan Nair AK, Cui R, Sun S (2021) Overview of the adsorption and transport properties of water, ions, carbon dioxide, and methane in swelling clays. ACS Earth Space Chem 5(10):2599–2611. https://doi.org/10.1021/acsearthspacechem.1c00160
36. Park S, Schulten K (2004) Calculating potentials of mean force from steered molecular dynamics simulations. J Chem Phys 120(13):5946–5961. https://doi.org/10.1063/1.1651473
37. Plimpton S (1995) Fast parallel algorithms for short-range molecular dynamics. J Comput Phys 117(1):1–19. https://doi.org/10.1006/jcph.1995.1039
38. Prasanth KP, Pillai RS, Bajaj HC, Jasra RV, Chung HD, Kim TH, Song SD (2008) Adsorption of hydrogen in nickel and rhodium exchanged zeolite X. Int J Hydrog Energy 33(2):735–745. https://doi.org/10.1016/j.ijhydene.2007.10.047
39. Rappe AK, Casewit CJ, Colwell KS, Goddard WA, Skiff WM (1992) Uff, a full periodic table force field for molecular mechanics and molecular dynamics simulations. J Am Chem Soc 114(25):10024–10035. https://doi.org/10.1021/ja00051a040
40. Saffer DM, Marone C (2003) Comparison of smectite- and illite-rich gouge frictional properties: application to the updip limit of the seismogenic zone along subduction megathrusts. Earth Planet Sci Lett 215(1–2):219–235. https://doi.org/10.1016/S0012-821X(03)00424-2
41. Sakuma H, Kawai K, Katayama I, Suehara S (2018) What is the origin of macroscopic friction? Sci Adv 4(12):2268. https://doi.org/10.1126/sciadv.aav2268
42. Sakuma H, Lockner DA, Solum J, Davatzes NC (2022) Friction in clay-bearing faults increases with the ionic radius of interlayer cations. Commun Earth Environ 3(1):116. https://doi.org/10.1038/s43247-022-00444-3
43. Smith DE, Dang LX (1994) Computer simulations of cesium-water clusters: do ion-water clusters form gas-phase clathrates? J Chem Phys 101(9):7873–7881. https://doi.org/10.1063/1.468213
44. Smith DE, Dang LX (1994) Computer simulations of nacl association in polarizable water. J Chem Phys 100(5):3757–3766. https://doi.org/10.1063/1.466363
45. Steinhauser O (1982) Computer simulation of polar liquids the influence of molecular shape. Mol Phys 46(4):827–837. https://doi.org/10.1080/00268978200101611
46. Stukowski A (2010) Visualization and analysis of atomistic simulation data with ovito–the open visualization tool. Model Simul Mater Sci Eng 18(1):15012. https://doi.org/10.1088/0965-0393/18/1/015012
47. Tan Z, Chen S (2006) Nucleic acid helix stability: effects of salt concentration, cation valence and size, and chain length. Biophys J 90(4):1175–1190. https://doi.org/10.1529/biophysj.105.070904
48. Tembe S, Lockner DA, Wong T (2010) Effect of clay content and mineralogy on frictional sliding behavior of simulated gouges: binary and ternary mixtures of quartz, illite, and montmorillonite. J Geophys Res. https://doi.org/10.1029/2009JB006383
49. Tetsuka H, Katayama I, Sakuma H, Tamura K (2018) Effects of humidity and interlayer cations on the frictional strength of montmorillonite. Earth Planets Space 70(1):56. https://doi.org/10.1186/s40623-018-0829-1

50. Tian K, Gosvami NN, Goldsby DL, Carpick RW (2018) Stick-slip instabilities for interfacial chemical bond-induced friction at the nanoscale. J Phys Chem B 122(2):991–999. https://doi.org/10.1021/acs.jpcb.7b09748
51. Tuan LH, Sang LV (2023) Annealing coatings of graphene on silicon and application to tribology. Tribol Int 185:108539. https://doi.org/10.1016/j.triboint.2023.108539
52. Ujiie K, Tanaka H, Saito T, Tsutsumi A, Mori JJ, Kameda J, Brodsky EE, Chester FM, Eguchi N, Toczko S (2013) Low coseismic shear stress on the Tohoku-Oki megathrust determined from laboratory experiments. Science 342(6163):1211–1214. https://doi.org/10.1126/science.1243485
53. Viani A, Gualtieri AF, Artioli G (2002) The nature of disorder in montmorillonite by simulation of X-ray powder patterns. Am Miner 87(7):966–975. https://doi.org/10.2138/am-2002-0720
54. Wan J, Zaoui A (2024) Mechanical resistance behind fiber-reinforced polymer pile: role of clay minerals. Comput Geotech 168:106158. https://doi.org/10.1016/j.compgeo.2024.106158
55. Wei P, Xiong Y, Zheng Y, Zaoui A, Yin Z, Niu W (2023) Nanoscale friction at the quartz–quartz/kaolinite interface. Colloids Surf A Physicochem Eng Asp 676:132296. https://doi.org/10.1016/j.colsurfa.2023.132296
56. Wei P, Zhang L, Zheng Y, Diao Q, Zhuang D, Yin Z (2021) Nanoscale friction characteristics of hydrated montmorillonites using molecular dynamics. Appl Clay Sci 210:106155. https://doi.org/10.1016/j.clay.2021.106155
57. Wei P, Zheng Y, Zaoui A (2024) Frictional mechanisms of hydrated montmorillonite under normal loading. Comput Geotech 173:106568. https://doi.org/10.1016/j.compgeo.2024.106568
58. Wei P, Zhou S, Zheng Y, Yin Z, Xu W (2024) Nanoscale stick-slip behavior and hydration of hydrated illite clay. Comput Geotech 166:105976. https://doi.org/10.1016/j.compgeo.2023.105976
59. Xu WQ, Yin ZY, Zheng YY (2023) FRP-soil interfacial mechanical properties with molecular dynamics simulations: insights into friction and creep behavior. Int J Numer Anal Methods Geomech. https://doi.org/10.1002/nag.3607
60. Xu W, Yin Z, Zheng Y (2023) Investigating silica interface rate-dependent friction behavior under dry and lubricated conditions with molecular dynamics. Acta Geotech 18(7):3543–3554. https://doi.org/10.1007/s11440-022-01792-2
61. Ying H, Pei H, Zhang S (2024) Investigation on the friction properties of montmorillonite by molecular dynamics considering the effects of water content, cation species, ion concentration and temperature. Comput Geotech 171:106345. https://doi.org/10.1016/j.compgeo.2024.106345
62. Zhang Q, Qi Y, Hector LG, Çağın T, Goddard WA (2005) Atomic simulations of kinetic friction and its velocity dependence at Al/Al and $A-Al_2O_3/A-Al_2O_3$ interfaces. Phys Rev B 72(4):45406. https://doi.org/10.1103/PhysRevB.72.045406